Charge transfer in $YBa_2Cu_3O_6$ doped with fluorine: Infrared reflectance and Raman scattering studies

A. Sacuto, C. Julien, and V. A. Shchukin*
Laboratoire de Physique des Solides, CNRS URA 154, Université Pierre et Marie Curie, Tour 13, E2, 4 Place Jussieu, 75252 Paris, Case 79, Cédex 05, France

C. Perrin and M. Mokhtari
Laboratoire de Chimie du Solide et Inorganique Moleculaire, CNRS URA 1495, Université de Rennes I, Avenue du Général Leclerc, 35042 Rennes, Cédex, France

(Received 24 October 1994; revised manuscript received 25 January 1995)

Charge transfer between the Cu-O chains and the Cu-O_2 planes has been studied by far infrared reflectivity (FIR) and Raman scattering (RS) measurements on $YBa_2Cu_3O_6F_y$ compounds with $0 \leq y \leq 1.46$. Analysis of the reflectivity spectra by the four parameter semiquantum model shows the occurrence of the insulator/metallic transition for $y = 0.76$, in agreement with the dc conductivity. The ω_{LO}-ω_{TO} frequency splittings related to the intralayer modes involving the atomic vibrations of the BaO and CuO_2 planes decrease, whereas the ω_{LO}-ω_{TO} splittings related to the interlayer modes, involving the atomic vibrations of the Cu2-O4-Cu1 bonding, increase. We discuss three possible reasons for the change of the LO-TO splitting with increased fluorine doping: (i) charge transfer between ions which changes effective ionic charges; (ii) effect of lattice disorder induced by the fluorine, and (iii) the effect of the plasma in ceramics. We show that the charge transfer assumption is more than likely and is consistent with both FIR and RS investigations. Raman spectra exhibit frequency hardening of the O4-Cu2 modes and frequency softening of the O2-O3 modes with increased fluorine doping. The former points out the increase of the Coulomb interactions between ions within the interlayer bonds and the latter, their decrease and screening inside the CuO_2 planes. The phonon line shape of the B_{1g} mode related to the CuO_2 planes changes with the fluorine doping. The phonon line shape depends on the electronic polarization operator (EPO) which has been related to the free-carrier density of the CuO_2 planes. The increase of the EPO points out the enhancement of the free-carrier density in the CuO_2 planes. The charge transfer is revealed by the increase of the ionic Coulomb interactions within the Cu1-O4-Cu2 interlayer bonds, and their decrease and screening by the free carriers enhancement inside the CuO_2 planes as fluorine doping increases.

I. INTRODUCTION

Since the discovery of YBCO high-T_c superconductors, many Raman and infrared measurements have been performed on $YBa_2Cu_3O_{6+x}$ compounds with variable oxygen content.[1-6] The main objective was to study, by a phonon analysis, the tetragonal/orthorhombic (T/O) and the insulator/metallic (I/M) phase transition which simultaneously occur with superconductivity at $x \approx 0.35$. The existence of a charge transfer between CuO chains and CuO_2 planes, via the BaO planes, is a current interpretation for the increase of the hole concentration in the CuO_2 planes and the I/M transition.[7-9] Optical conductivity measurements show that the mobile carrier spectral weight is redistributed from the charge-transfer band region of the insulating $YBa_2Cu_3O_6$ to low frequencies as the doping is increasing.[10] The low-frequency conductivity associated with the CuO_2 planes exhibits a non-Drude response. On the contrary, the interplanar optical response of highly doped YBCO is characterized by a Drude-like behavior.[10,11] Neutron-powder-diffraction measurements show a significant change in the Cu1-O4-Cu2 and Cu2-Cu2 bond lengths near $x \approx 0.35$, which could be consistent with a charge transfer.[12,13] Unfortunately, the occurrence of the T/O transition at the same oxygen concentration sheds some doubt on the origin of these structural parameter changes. The simultaneous occurrence of the I/M and the T/O transitions, and the difficulty in synthesizing a large number of samples with low oxygen content between $0 \leq x \leq 0.4$, are the two main reasons why charge transfer has not been clearly detected by a phonon analysis in the $YBa_2Cu_3O_{6+x}$ compounds.

In this paper, we propose to detect and study, by a far-infrared reflectance (FIR) and a Raman scattering (RS) analysis on the electronic excitations, the phonons, and their interactions, the charge transfer and the I/M transition which we show to occur as fluorine atoms are inserted into Cu1-Cu1 chains of the $YBa_2Cu_3O_6$ matrix. Fluorine insertion is another way to reach the metallic superconducting state from the $YBa_2Cu_3O_6$ structure with the advantage of preserving the tetragonal phase during fluorination and to exhibit an I/M transition at high fluorine content, $y \approx 0.76$ ($y \approx 2x$).

By fitting the experimental reflectivity spectra to the theoretical reflectance function obtained from the four

parameter semiquantum (FPSQ) model, we have determined the evolution of the free-carrier density and the FIR active normal modes as functions of the fluorine content.[14] Strong enhancement of the plasma frequency near $y \approx 0.76$ shows the occurrence of the I/M transition at this fluorine content. The ω_{LO}-ω_{TO} frequency splitting related to the intralayer modes of the BaO and CuO_2 planes decreases with increasing y, whereas the ω_{LO}-ω_{TO} splitting related to the interlayer modes of the Cu2-O4 bonding increases. We examine three possible reasons for the change of the LO-TO splitting with increasing fluorine doping: (i) the charge transfer between ions which changes the effective ions charges; (ii) the effect of lattice disorder induced by the insertion of the fluorine atoms into the $YBa_2Cu_3O_6$ matrix; and (iii) the effect of the plasma in ceramics, (i.e., the effect of the plasma energy variation in a dilute system of crystalline inclusions embedded into a matrix). We show that the two last effects are insufficient to explain the changes of the ω_{LO}-ω_{TO} splitting detected with doping increase, whereas the charge-transfer assumption is more than likely and consistent with FIR and RS measurements. Analysis of the Raman phonon energy shifts have permitted us to point out the increase of the effective Coulomb forces within the Cu2-O4 bond and their decrease inside the CuO_2 planes. We develop an analysis of the deformation of the B_{1g} normal mode line shape related to the oxygen vibrations of the CuO_2 planes. The electronic polarization operator (EPO), deduced from the phonon line-shape calculation, is found to be proportional to the free-carrier density of the CuO_2 planes. The EPO increases with fluorine doping. This agrees with the enhancement of the free-carrier density in the CuO_2 planes. The charge transfer is revealed by an increase of the ionic Coulombic interactions within the Cu1-O4-Cu2 interlayer bonds and their decrease and screening by free-carrier enhancement inside the CuO_2 planes as fluorine doping increases.

The sample preparation and characterization by x-ray diffraction, magnetic susceptibility, and dc conductivity measurements are given in Sec. II. The FIR and RS experimental techniques are described in Sec. III. The FIR and RS investigations are developed in Secs. IV and V, respectively.

II. SAMPLE PREPARATION AND CHARACTERIZATION

The $YBa_2Cu_3O_6$ starting samples were synthesized from stoichiometric amounts of Y_2O_3, $BaCO_3$, and CuO heated for 2 h at 970 °C in an alumina boat and quenched in air. The powder obtained was reground. Many identical pellets (diameter =6 mm, thickness =2 mm, mass =200 mg) pressed at a uniaxial pressure of 1 kbar were sintered for 2 h at 970 °C and air quenched. The samples were then heated at about 700 °C under a dynamic vacuum for several hours in order to obtain the tetragonal phase. Series of samples were then heated under an NF_3 flow at 320 °C for various periods of time given in Table I. More details of the thermal treatment are given elsewhere.[15–17] During fluorination, the $YBa_2Cu_3O_6F_y$ structure remains tetragonal. Indeed x-ray-diffraction measurements show no evidence of a T/O phase transition in contrast to the $YBa_2Cu_3O_{6+x}$ structure during oxygenation. The lattice parameters as a function of fluorine content are listed in Table I. The "a" parameter increases smoothly with fluorine doping while the "c" parameter decreases for fluorine content higher than $y=0.17$. Evidence for fluorine insertion was first given by a classical chemical test using alizarine.[15] Thermogravimetric measurements have confirmed the presence of fluorine in the pellets and the sample analysis carried out with an energy dispersive spectrometer (EDS) coupled to a scanning microscope have permitted us to detect the presence of fluorine in the microcrystallites of the pellets.[17] Conservation of the tetragonal structure confirms the equiprobable repartition of the fluorine atoms into the O1 and O5 sites. The $YBa_2Cu_3O_6F_y$ structure is shown in Fig. 1. Neutron-powder-diffraction measurement reveal the insertion of fluorine atoms inside the Cu1-Cu1 chains.[15–17] The critical temperatures, T_c, have been obtained by magnetic susceptibility measurements. The transition onsets, T_c^{onset}, are reported in Table I; the typical transition width is $\Delta T_c \approx 7$ K. The superconductivity occurs in the metallic phase ($y \geq 0.76$). The T_c^{onset} increases with the fluorine doping from $y=0.76$ to 1.26, and then exhibits a maximum "plateau" near 55 K. The T_c^{onset} behavior for $0 \leq y \leq 0.1.46$ is similar to the T_c^{onset} behavior of $YBa_2Cu_3O_{6+x}$ for $0 \leq x \leq 0.7$.

TABLE I. Times of fluorination process, lattice parameters, and T_c versus fluorine doping. Estimates of errors for the lattice parameters on the last decimal are given in parentheses.

		Parameters (Å)		
$YBa_2Cu_3O_6F_y$	Time (mn)	a	c	T_c^{onset} (K)
$y=0.00$	0	3.847(1)	11.795(1)	
$y=0.17$	15	3.857(1)	11.801(1)	
$y=0.38$	30	3.860(2)	11.772(3)	
$y=0.76$	60	3.863(1)	11.745(2)	35
$y=1.11$	180	3.867(1)	11.739(2)	45
$y=1.26$	300	3.868(1)	11.715(3)	55
$y=1.46$	480	3.871(1)	11.709(2)	55

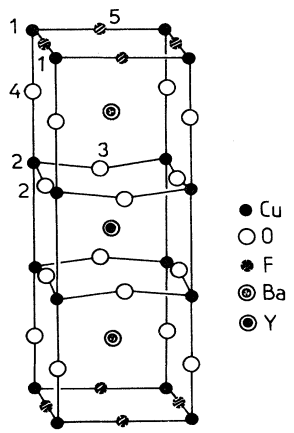

FIG. 1. The $YBa_2Cu_3O_6F_y$ structure.

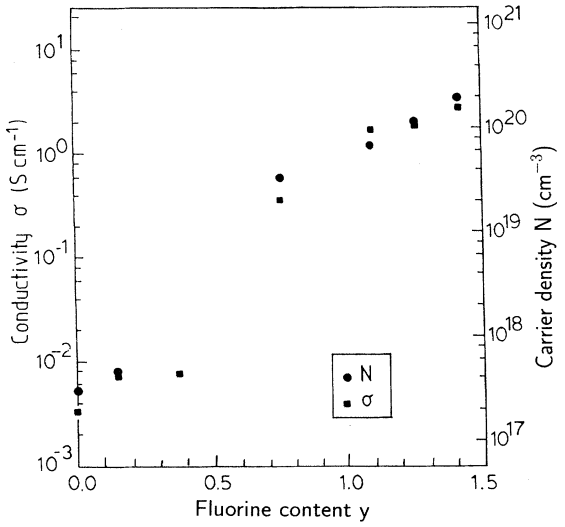

FIG. 2. dc conductivity σ, obtained from the resistivity measurements and free-carrier density N, obtained from the fits of the FPSQ model to the FIR spectra with various fluorine content, $T=300$ K.

Resistivity measurements have been performed at room temperature on the $YBa_2Cu_3O_6F_y$ compounds using the Van der Pauw method.[17] Four indium contacts were ultrasonically soldered on the sample and the dc conductivity at room temperature as a function of fluorine content is represented in Fig. 2. The conductivity shows a sharp and strong enhancement of two orders of magnitude around $y\approx 0.76$, which suggests a drastic increase of the free-carrier density in $YBa_2Cu_3O_6F_y$ compounds. The $YBa_2Cu_3O_6F_y$ conductivity is of the same order of magnitude as that in $YBa_2Cu_3O_{6+x}$ ceramics.

III. EXPERIMENTAL ARRANGEMENT

The far-infrared-reflectivity (FIR) measurements have been performed with a Bruker IFS 113 vacuum Fourier transform spectrometer, equipped with a liquid-helium-cooled Ge bolometer and a 6 μm thick Mylar beam splitter. Each spectrum is the average of 100 scans recorded with a spectral resolution of 2 cm^{-1} using a quasispecular reflection unit working at an incident angle of 11°. The reflectivity reference spectrum was obtained using a bulk-gold mirror; the uncertainty in reflectivity is $\Delta R=\pm 0.01$. The surface of the sintered pellets was polished using diamond pasts of 1, 0.5, and 0.1 μm and petroleum spirit containing less than 0.01% water. FIR spectra were obtained from randomly oriented crystallites at the surface of the pellets.

Micro-Raman scattering (MRS) measurements have been carried out at room temperature with a U-1000 Jobin Yvoin double monochromator using the 514.52 nm line of an argon-ion laser. A photomultiplier tube EMI 9863B was connected to a microcomputer for data collection. A microprobe in conjunction with the spectrometer produces a laser spot of a few square micrometers. A video camera, connected to the microprobe, allowed us to observe and focus the laser beam on the surface of a single crystallite. The incident and scattered light were focused and collected by the microprobe objective, leading to a perfect backscattering geometry. Orientation of the crystallite has been chosen, such as, the incident and scattered electric fields are parallel and contained in the (xy) plane of the crystallite. The electric polarization are denoted x' [x' does not have a particular axis orientation in the (xy) plane]. The instrumental resolution was $\Delta=0.5$ cm^{-1}. The intensity was maintained below roughly 10 W/cm^2 in order to minimize possible thermal damage on the sample surface.

IV. INFRARED MEASUREMENTS

FIR measurements on $YBa_2Cu_3O_6F_y$ compounds ($y=0$, 0.17, 0.76, 1.11, 1.26, and 1.46) between 10 and 1000 cm^{-1} are shown in Fig. 3. The reflectivity spectra exhibit distinct structures which are attributed to the presence of phonon absorptions. These structures are clearly smeared with the fluorine doping at $y\geq 0.76$. Simultaneously, the reflectance increases significantly, starting from $R(\omega)\approx 0.3$ for $y=0$ at $\omega=100$ cm^{-1} to reach $R(\omega)\approx 0.8$ for $y=1.46$, a typical value for a metallic YBCO pellet.[18–20] The enhancement of the reflectivity background and the smearing of the phonon structures are highly suggestive of the presence of free carrier. Therefore the quantitative phonon analysis in the

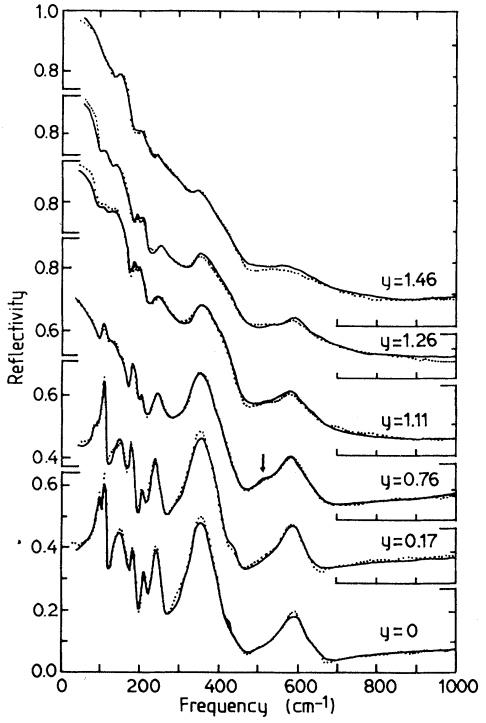

FIG. 3. FIR measurements on $YBa_2Cu_3O_6F_y$ with various fluorine contents, $T=300$ K. The experimental curves are represented by dashed lines and the full lines represent the theoretical curves obtained from the FPSQ model.

$YBa_2Cu_3O_6F_y$ compounds has been restricted to $y \leq 0.76$.

In order to estimate the evolution of the free-carrier density and the transverse and longitudinal optical frequencies, ω_{TO} and ω_{LO}, associated with the vibrational modes of $YBa_2Cu_3O_6F_y$, we have fitted the experimental spectra. The theoretical reflectivity function was obtained from the FPSQ model.[14] The reflectance $R(\omega)$ is related to the complex dielectric function $\varepsilon^*(\omega)$:

$$R(\omega)=\{[n^*(\omega)-1]/[n^*(\omega)+1]\}^2 , \quad (1)$$

with the complex refractive index

$$n^*(\omega)=[\varepsilon^*(\omega)]^{1/2} . \quad (2)$$

In this model, the complex dielectric function is given by

$$\varepsilon^*=\varepsilon_\infty \left[\prod_i \frac{\omega_{L,i}^2-\omega^2-i\omega\gamma_{L,i}}{\omega_{T,i}^2-\omega^2-i\omega\gamma_{T,i}} - \frac{\bar{\omega}_p^2-i\omega(\gamma_p-\gamma_0)}{\omega^2+i\omega\gamma_0} \right] . \quad (3)$$

The first term in the brackets represents the phonon contribution while the second corresponds to the free-electron contribution. ε_∞ is the high-frequency dielectric function. $\omega_{L,i}$ ($\omega_{T,i}$) and $\gamma_{L,i}$, ($\gamma_{T,i}$) are the longitudinal (transverse) optical frequencies and damping of the normal mode i, respectively. $\bar{\omega}_p$ is the plasma frequency which does not include ε_∞. Usually, ε_∞ is included in the plasma frequency denoted ω_p.[18,21–24] Here, $\omega_p^2=\varepsilon_\infty\bar{\omega}_p^2$. γ_p represents the plasma damping, and γ_0 the damping at zero frequency. γ_0 may be different from γ_p because the relaxation times of the electrons are usually different at low and high frequencies. On the contrary, in the Drude model, the plasmon damping is considered a constant. The Drude equation is obtained when $\gamma_0=\gamma_p$. The fit of $R(\omega)$ was done using a modified Gauss-Newton nonlinear least-squares estimation technique. A computed reflectivity is considered to fit satisfactorily if it departs by less than $\pm 2\%$ from the experimental spectrum. We accept local differences of $\pm 2\%$, but not overall deviations. The infrared data of the high-T_c superconductors have been analyzed in terms of a non-Drude behavior at low frequency, and a so-called midinfrared band (MIB) at high frequency.[21–24] The infrared response at low frequency is described by a generalized Drude response where at least one term, either the scattering rate or the effective mass, is frequency dependent.[21–24] In the FPSQ model, we have taken into account the frequency dependence of the scattering rate by considering the monotonical variation of the plasma damping function from γ_0 to γ_p, but we have not explicitly taken into account the MIB contribution. The frequency dependence of the plasma damping and the appearance of the MIB for high doped fluorine ($y \geq 0.76$) can strongly undetermine the accuracy of the $\bar{\omega}_p$ and ε_∞ parameters. One can decrease $\bar{\omega}_p$ and balance this decrease by increasing the plasma damping difference $(\gamma_p-\gamma_0)$ and conversely without changing significantly the shape of the spectrum. Concerning our fit, we have chosen to reduce the $(\gamma_p-\gamma_0)$ difference as it is possible, and keep γ_p and γ_0 of the same order. The theoretical curve is represented by the full lie in Fig. 3. The agreement between the model and the experimental spectra is quite good between 10 and 1000 cm^{-1}, because we have taken into account the dampings of the LO and TO modes, and the variation of the plasma damping with frequency.

The plasma frequencies, $\bar{\omega}_p$, ω_p, the γ_0 and γ_p damping, and the high-frequency dielectric function, ε_∞, obtained from these fits are given in Table II. The plasma frequencies, ω_p, of the metallic $YBa_2Cu_3O_6F_y$ compounds are similar to the plasma frequencies obtained from the metallic $YBa_2Cu_3O_{6+x}$ polished ceramics with the same T_c.[22] However, it is difficult to clearly estimate the plasma frequencies because, as evident from Table II, the plasma, obtained from the FPSQ model, is overdamped. This overdamping has also been observed in the conducting oxides and $YBa_2Cu_3O_7$ high-T_c superconductors.[25,26] These high damping values (compared with $\bar{\omega}_p$) have been interpreted as evidence of a strong interaction between charge carriers and some excitations.[26] We notice in Table II a decrease of ε_∞ with the fluorine doping. This can be explained by the redistribution of the MIB of the insulating phase (centered near 1.5 eV) to low frequencies as the doping increases.[10] Indeed, for $y=0$, at high frequency, the expression of the dielectric function (without damping) deduced from the FPSQ model is given by $\varepsilon(\omega)=\varepsilon_\infty(1-\bar{\omega}_p^2/\omega^2)\approx\varepsilon_\infty$. For high doping levels, if we take into account the MIB contribution and define it by the simplest expression, $\omega_f^2/(\omega_0^2-\omega^2)$, where ω_0 is the frequency of the centered band, and ω_f, the Lorentz oscillator strength, the dielectric function becomes at high frequency ($\omega \gg \bar{\omega}_p$, $\omega \gg \omega_0$ and $\omega_f \gg \omega_p$), $\varepsilon(\omega)\approx\varepsilon_\infty-\omega_f^2/\omega^2$. This expression shows that the MIB contribution can actually decrease the ε_∞ value.

The free-carrier density in the simple Drude model, for the case of one type of carriers, is defined by $N=(\bar{\omega}_p^2 m^* \varepsilon_\infty)/4\pi e^2$. m^* and e represent the electron effective mass and charge, respectively (m^* has been taken equal to the bare electron mass). The free-carrier density variation, as the fluorine content increases, is shown in Fig. 2. Its behavior is similar to that of the dc conductivity and shows a drastic enhancement around $y \approx 0.76$ which we relate to the I/M transition. The ω_{TO} and ω_{LO} frequencies related to the normal modes of the $YBa_3Cu_3O_6F_y$ structure are listed in Table III. The

TABLE II. Plasma frequencies, $\bar{\omega}_p$, ω_p, plasmon dampings γ_0,γ_p, and high-frequency dielectric functions, ε_∞, obtained from the fits of the FPSQ model to the FIR spectra with various fluorine contents. Estimates of errors of the fitted parameters are given in parentheses.

y	0.00	0.17	0.76	1.11	1.26	1.46
$\bar{\omega}_p$ (cm^{-1})	85(1)	100(1)	964(1)	1404(1)	1922(1)	2650(1)
γ_0 (cm^{-1})	151(1)	154(1)	1347(1)	3590(1)	4420(1)	5610(1)
γ_p (cm^{-1})	156(1)	164(1)	1360(1)	3627(1)	4502(1)	5720(1)
ω_p (cm^{-1})	160±3	190±2	1564±8	2350±10	3038±14	4190±19
ε_∞	3.5(2)	3.6(2)	2.6(2)	2.8(2)	2.5(2)	2.5(2)

γ_{TO},γ_{LO} damping values correspond to 2% of ω_{TO} and ω_{LO} for $y=0$ and 0.17, and increase to 4% of ω_{TO} and ω_{LO} for $y=0.76$. The assignment of the atomic groups involved in each normal mode (see Table III) are deduced from lattice dynamical calculations and previous FIR analyses performed on $YBa_2Cu_3O_6$.[19,20,27,28]

At $y=0$, $YBa_2Cu_3O_6$ has 11 infrared active modes which transform as $5A_u+6E_u$ irreducible representations of the D_{4h} point group. The five expected A_{2u} modes are detected, whereas five of the six predicted E_u modes are observed.[19,20,27,28] As the fluorine content increases, the normal modes related to $YBa_2Cu_3O_6$ shift in frequency or gradually disappear due to screening by the increasing charge density. We note in Table III the occurrence of a new mode at $\omega_{TO}=483.2$ cm^{-1} which does not belong to $YBa_2Cu_3O_6$. Although we have not performed a polarized infrared analysis, we suggest that this mode is similar to the B_{1u} normal mode of $YBa_2Cu_3O_7$ representing the Cu1-O1 bond bending along the "c" axis.[29] We assign it to the Cu1-F bond bending along the c axis. Its frequency is lower than that for $YBa_2Cu_3O_7$, because the atomic fluorine mass is greater than the oxygen mass. This vibrational mode is pointed out by an arrow on the $y=0.76$ spectrum in Fig. 3.

A striking feature in Table III is the increase and decrease of the ω_{LO}-ω_{TO} frequency splitting related to the A_{2u} and E_u normal modes, respectively, as the fluorine atoms are inserted into $YBa_2Cu_3O_6$. This is valid for all the modes except for the Y-E_u mode. The ω_{LO}-ω_{TO} splitting of all the normal modes is strongly altered at the I/M transition. One can identify three possible reasons for the change of LO-TO splitting with the increase of the fluorine concentration: (i) the charge transfer between ions which changes the effective ion charges; (ii) lattice dynamics of an imperfect lattice; and (iii) the effect of plasma in ceramics. First, we discuss the charge transfer between ions and the effects of disorder due to fluorine atom insertion. FIR measurements on the pellets give both (xy)-plane and z-axis contributions of the electric fields.

For (xy)-plane contribution, the Lyddane-Sachs-Teller (LST) relation, valid for any number of atoms in the unit cell of a tetragonal structure, is given by[29]

$$\prod_j \left[\frac{\omega_{L,j}(E_u)}{\omega_{T,j}(E_u)}\right]^2=\frac{\varepsilon_0^{xx}}{\varepsilon_\infty^{xx}} . \tag{4}$$

The (xy)-plane contribution of the incident electric field couples to the modes of E_u symmetry. ε_0 is the static dielectric function and $\varepsilon_0^{xx}/\varepsilon_\infty^{xx}=4\pi\chi_{vib}^{xx}/(1+4\pi\chi_{elec}^{xx})$, where χ_{vib} and χ_{elec} are the susceptibilities related to the ionic vibrations and the bound electrons, respectively (the LST relation does not take into account the free-electron contribution). The LST formula shows that the ω_{LO}-ω_{TO} splitting related to the E_u modes decreases when χ_{vib} decreases or (and) χ_{elec} increases in the Ba-O and CuO_2 planes. Similarly, the increase of the ω_{LO}-ω_{TO} frequency splitting related to the A_{2u} modes is due to an increase of χ_{vib} or (and) decrease of χ_{elec}. The decrease of χ_{elec} for the A_{2u} modes indicates an enhancement of the interlayer bond ionicity along the c axis, whereas the χ_{elec} increase for the E_u modes is related to enhancement of the covalent bond character in the Ba-O and Cu-O_2 planes during fluorination. The susceptibility of χ_{vib} is sensitive to local disorder inside the structure and thus sensitive to the fluorine atom insertion. At this step of the discussion, it is difficult to conclude and define what is the effect (charge transfer or imperfect lattice) responsible for the LO-TO splitting. However, it seems unlikely that any

TABLE III. ω_{TO}-ω_{LO} frequencies of each normal mode deduced from the fits of the FPSQ model to the FIR spectra with various fluorine contents. Frequencies are in cm^{-1} and the estimates of errors of the fitted parameters are given in parentheses.

			A_{2u} normal modes (interlayer modes)			
$y=0$		$y=0.17$		$y=0.76$		
ω_{TO}	ω_{LO}	ω_{TO}	ω_{LO}	ω_{TO}	ω_{LO}	Assignments
103.0(2)	106.5(2)	100.4(2)	107.0(2)	103.2(2)	115.3(2)	Ba translation along c
152.1(2)	175.0(2)	152.5(2)	176.1(2)	150.0(2)	180.3(2)	O4-Cu1-O4 translation along c
213.0(2)	218.0(2)	211.2(2)	216.2(2)	186.1(2)	203.3(2)	Y translation along c
445.1(2)	449.0(2)	441.0(2)	446.1(2)			Cu2-O2 bond bending along c
653.5(2)	658.9(2)	651.0(2)	659.2(2)	645.1(2)	667.1(2)	Cu1-O4 bond stretching along c
			E_u normal modes (intralayer modes)			
114.0(2)	121.0(2)	114.1(2)	121.2(2)	115.1(2)	116.1(2)	Ba translation in ab plane Cu1 translation in ab plane
185.1(2)	194.2(2)	184.0(2)	195.1(2)	183.2(2)	198.4(2)	Y translation in ab plane
240.0(2)	259.0(2)	242.1(2)	259.5(2)	256.6(2)	257.5(2)	O4-Cu1 bond bending in ab plane
341.0(2)	415.0(2)	341.3(2)	415.1(2)	343.5(2)	366.2(2)	O2-Cu2 bond bending in ab plane
592.0(2)	622.1(2)	591.1(2)	621.2(2)	580.6(2)	599.5(2)	Cu2-O2 bond stretching in ab plane
			New mode			
			483.2(2)	485.3(2)		Cu1-F bond bending along c

atomic disorder due to the fluorine insertion into the chains produces, on one hand, an increase of the LO-TO splitting of the interlayer modes while, on the other, decreases the LO-TO splitting of the intralayer modes.

We discuss now, in some detail, the effect of the plasma in ceramics. We model the ceramic as a dilute system of crystalline inclusions embedded into a matrix with an effective dielectric constant ε_M^{xx}. All inclusions are assumed to have the shape of an oblate spheroid with semiaxes $a=b$ and $c \ll a$. Then the effective dielectric function of the system is equal to[30]

$$\varepsilon_{\text{eff}}^{xx}(\omega)=\varepsilon_M^{xx}+p\left[(1-\gamma)\frac{\varepsilon^{xx}(\omega)-1}{1+n^x[\varepsilon^{xx}(\omega)-1]}+\gamma\frac{\varepsilon^{zz}(\omega)-1}{1+n^z[\varepsilon^{zz}(\omega)-1]}\right]. \quad (5)$$

Here $\varepsilon^{xx}(\omega)$ and $\varepsilon^{zz}(\omega)$ are the components of the tensor of crystalline inclusions; $n^x=(\pi/4)(c/a)$, and $n^z=1-(\pi/2)(c/a)$ are the depolarization factors of spheroids, and p is the concentration of inclusions varying between 0 and 1. The factor γ describes the distribution of the orientation of inclusions. If all inclusions lie in the (xy) plane, $\gamma=0$; if the distribution is random, $\gamma=\frac{1}{3}$.

To emphasize the difference between the dielectric function used for the fit [Eq. (3)] without damping and that of Eq. (5), we take the simplest model for the dielectric function of crystallites,

$$\varepsilon^{xx}(\omega)=\varepsilon_\infty^{xx}[(\omega_{\text{LO}}^2(E_u)-\omega^2)(\omega_{\text{TO}}^2(E_u)-\omega^2)^{-1}-\bar{\omega}_p^2\omega^{-2}], \quad (6)$$

and neglect the contribution of vibration along the z axis. The $\varepsilon^{xx}(\omega)$ expression given by Eq. (6) is inserted into Eq. (5). A comparison between Eqs. (3) and (5) yields

$$\Delta^{FIT}=\Delta-\frac{A}{2(A+1)}([\bar{\omega}_p^2+\Delta-(A+1)\omega_{\text{TO}}^2(E_u)]+\{[\bar{\omega}_p^2+\Delta-(A+1)\omega_{\text{TO}}^2(E_u)]^2+4(A+1)\Delta\omega_{\text{TO}}^2(E_u)\}^{1/2}). \quad (7)$$

Here $\Delta=\omega_{\text{LO}}^2(E_u)-\omega_{\text{TO}}^2(E_u)$ and $A=[\varepsilon_M^{xx}/(p(1-\gamma))]-1>0$. The quantity Δ^{FIT} is the LO-TO splitting, obtained by using Eq. (3) without damping. From Eq. (7), it follows that the value of the splitting Δ^{FIT} decreases with increasing plasma frequency $\bar{\omega}_p$. For weak dampings, this effect remains valid. The plasma effect in ceramics can explain the reduction of the LO-TO splitting of the E_u modes but cannot explain the increase of the LO-TO splitting of the A_{2u} modes. To eliminate this plasma effect in ceramics, optical measurements on c-axis-oriented thin films doped with fluorine are in progress.

V. RAMAN MEASUREMENTS

The Raman spectra of $YBa_2Cu_3O_6F_y$ pellets (with $y=0$, 0.17, 0.38, 0.76, 1.11, 1.26, 1.46) in the $Z(x'x')Z$ configuration are displayed in Fig. 4. For $y=0$, we observe three Raman-active modes among the five modes theoretically expected for the $YBa_2Cu_3O_6$ structure.[1–6] The peak located at 139.5 cm^{-1} has been assigned to the A_g mode corresponding to the vertical motion along the c axis of the Cu2 atoms and the peak at 338.5 cm^{-1} to the B_{1g} mode related to the O2-O3 oxygen vibrating out of phase along the c axis.[1–6] The peak at 452 cm^{-1} is actually a superposition of two modes, as inferred from the spectra of compounds with increasing fluorine doping. These two modes of A_g symmetry correspond to the motions of the O2-O3 oxygens and the O4 oxygen vibrating in phase along the c axis.[1–6]

As the fluorine atoms are inserted into $YBa_2Cu_3O_6$, the intensity of the B_{1g} mode at 338.5 cm^{-1} and the A_g mode at 139.5 cm^{-1} significantly decreases, their line shapes become asymmetric and their full width at half maximum (FWHM) increases. The B_{1g} and A_g modes re-

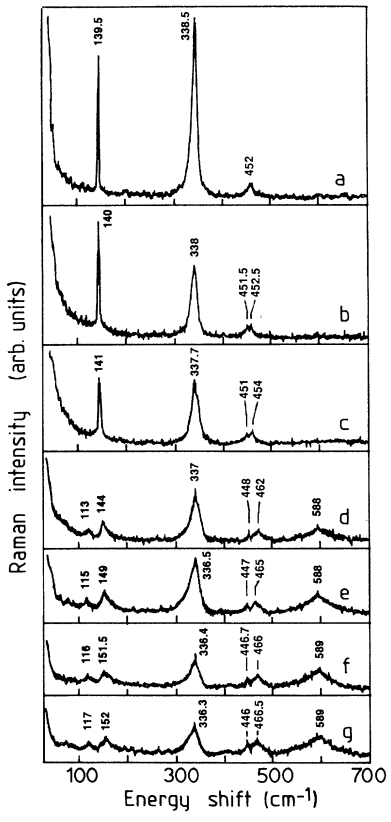

FIG. 4. RS spectra of the $YBa_2Cu_3O_6F_y$ with variable fluorine content in the $Z(x'x')Z$ configuration, $T=300$ K. (a) $y=0$, (b) $y=0.17$, (c) $y=0.38$, (d) $y=0.76$, (e) $y=1.11$, (f) $y=1.26$, (g) $y=1.46$.

lated to the O2-O3 oxygen atoms of the CuO_2 plane shift towards the low-frequency side, whereas the two A_g modes related to the Cu2-O4 bond stiffen. For intermediate fluorine content, two new bands centered at 113 and 588 cm^{-1} appear. The first one has been assigned to the normal mode related to the vertical motion of the barium atoms along the c axis and the second one does not belong to an eigenmode of either the $YBa_2Cu_3O_6$ tetragonal or the $YBa_2Cu_3O_7$ orthorhombic structures.[1-6] This large band usually appears in the spectra of $YBa_3Cu_3O_{6+x}$ structures when the oxygen deficiency in the Cu-O_x chains induces a symmetry lowering, or an ordering of the new oxygen vacancies similar to the one detected in the ortho-II phase.[6] This mode was assigned to the horizontal motion in the CuO_2 planes of the O3 oxygen atoms and is similar to the E_u infrared-active mode of the $YBa_2Cu_3O_6$ structure. In our case, this mode corresponds to a symmetry lowering induced by the insertion of fluorine atoms between two Cu1 sites. The presence of this mode is consistent with the insertion of fluorine into the $YBa_2Cu_3O_6$ structure, in the same manner as the observation of the infrared vibrational mode at $\omega_{TO}=485$ cm^{-1} (Table III).

The frequency shifts of the A_g modes and the B_{1g} mode accompanying the fluorine insertion are represented in Fig. 5. The Cu2 and the O4 normal modes both present a similar hardening in frequency, whereas the O2-O3 normal modes vibrating in phase and out of phase soften. For all modes, strong changes in frequency appear in the vicinity of $y=0.76$. The barium mode becomes Raman active beyond $y=0.76$. The Cu2 and O4 modes exhibit a strong hardening near $y=0.76$ at the I/M transition. Then it is possible to detect changes of the interlayer vibrational normal modes associated to the Cu1-O4-Cu2 bonds at the I/M transition. Significant modifications of the $YBa_2Cu_3O_{6+x}$ phonon spectrum at the I/M transition have not been detected unambiguously.[31] The two main reasons were the coincidence of the I/M and T/O transitions and the reduced interval of sample concentrations between $0\leq x\leq 0.4$. The hardening of the Cu2 and O4 normal mode and the softening of the O2-O3 modes are consistent with the charge-transfer hypothesis described in the FIR previous section. The ionic character of the interlayer bonds increases and the ionic Coulomb interactions are screened inside the BaO and CuO_2 planes. The frequency shift of the apical O4 mode with the charge redistribution in the 123 systems has also been reported from Raman investigations on $(YBa_2Cu_3O_7)_m/(PrBa_2Cu_3O_7)_n$ superlattices.[32,33] The absence of the barium normal mode in RS spectra below $y=0.76$ and its occurrence above $y\geq 0.76$ is not understood; it could be related to the local perturbation of the electronic polarization in the BaO plane at the I/M transition.

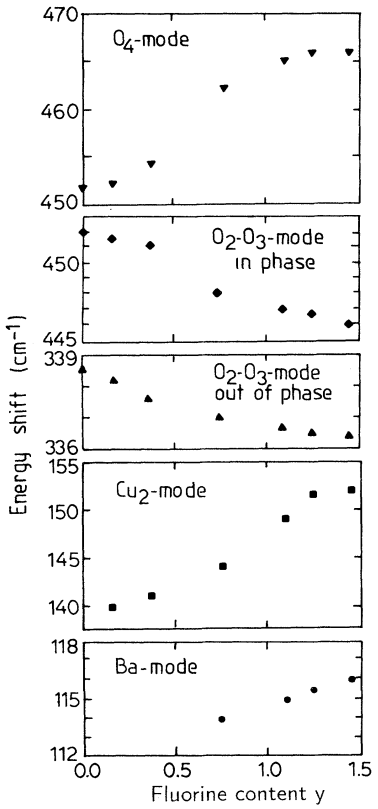

FIG. 5. Frequency shifts of the A_{1g} and B_{1g} modes with various fluorine contents in $YBa_2Cu_3O_6F_y$.

In order to study the free-carrier density fluctuations and show that the screening of the Coulombian interactions inside the CuO_2 plane is mainly due to increase of the free carrier with increasing fluorine doping, we now focus on the line-shape deformation of the B_{1g} mode of the CuO_2 plane with the fluorine doping. Different effects can produce a phonon asymmetric line shape (PAL). The two main effects are the interaction between a single phonon and an electronic continuum and the finite wave vector excitations which participate in Raman scattering. The finite wave vector excitations are coming from lack of translation invariance induced by lattice disorder. Two PAL's are detected in the Raman spectra [Fig. 4(d)], the first one at 144 cm^{-1} and the second at 337 cm^{-1}. These two phonons involve vibrations related to the CuO_2 planes. We shall study the second one, which exhibits the most intense Raman peak and corresponds to the B_{1g} mode. A detailed analysis of the finite wave vector phonon Raman process has shown that Raman scattering by B_{1g} phonons is less sensitive to disorder than that by A_{1g} modes.[34] The FWHM increase due to the disorder can then be neglected for the B_{1g} modes. The backscattering geometry, described in Sec. III, gives the z direction for the phonon wave vector. Therefore, no significant asymmetric line shape due to finite wave vector is expected for the mode at 337 cm^{-1} because its dispersion curve is flat along the Γ-Z symmetry line at the Brillouin zone center.[35] For these reasons, we suspect that the PAL of the B_{1g} mode results from the interaction of the B_{1g} phonon with an electronic continuum of the same symmetry. The Raman scattering intensity associated with an interference between a single phonon and an electronic continuum is given by[36-39]

$$I(\omega)=I_0\rho(\omega)\lambda^2\frac{(q+\varepsilon)^2}{1+\varepsilon^2}[n(\omega,T)+1]\ , \tag{8}$$

with

$$q=1/\lambda g\rho(\omega)\ , \tag{9}$$

$$\varepsilon=(\omega-\omega_0)/\Gamma\ , \tag{10}$$

$$\Gamma=g^2\rho(\omega)\omega_0\ , \tag{11}$$

and the Bose factor $n(\omega,T)=[\exp(\hbar\omega/k_BT)-1]^{-1}$. I_0 is an intensity factor which takes into account the intensity change due to the absorption coefficient variation of the material as fluorine is inserted into $YBa_2Cu_3O_6$ and the microcrystallite surface quality. ω_0 is the frequency of the bare phonon, g is the dimensionless electron-phonon (e-ph) coupling constant, and λ is the intensity ratio between the electron and phonon Raman scattering. Let us denote by $\Pi(\omega)$, the electronic polarization operator. $\rho(\omega)$ is related to the EPO by $\rho(\omega)=A\omega\,\mathrm{Im}[\Pi(\omega)]$. A is a dimensionless constant of proportionality and the imaginary part of the EPO represents the number of electronic excitations per unit frequency interval $(\omega,\omega+d\omega)$.

We have only considered the imaginary part of the EPO because the optical phonon energy falls inside the electron-hole continuum. The energy range of interest extends over the PAL centered at 337 cm^{-1}, e.g., 300–380 cm^{-1}. This allows us to consider $\rho(\omega)$ as a constant

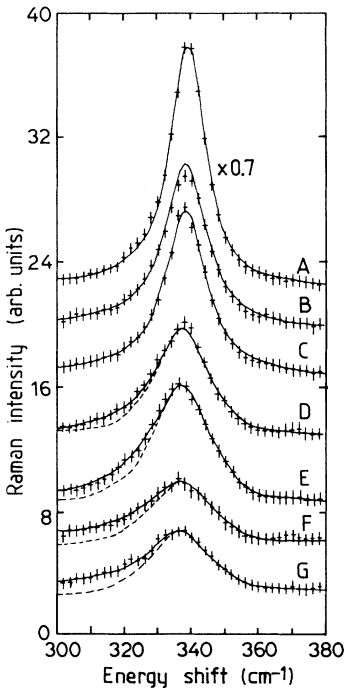

FIG. 6. PAL of the B_{1g} mode with various fluorine contents. The crosses represent the experimental data and the full lines represent the theoretical curves related to Eq. (7).

TABLE IV. The frequency of the pure phonon, ω_0, the intensity factor, I_0, the intensity ratio, λ, and the line-shape symmetric factor, q, obtained from the fit of Eq. (7) to the RS spectra with various fluorine contents. Estimates of errors of the fitted parameters are given in parentheses.

$YBa_2Cu_3O_6F_y$	ω_0 (cm^{-1})	I_0	λ	$\lvert q\rvert$
$y=0.00$	339.0(1)	0.421(1)	0.317(1)	35.210(1)
$y=0.17$	338.5(1)	0.226(1)	0.335(1)	30.302(1)
$y=0.76$	338.0(1)	0.204(1)	0.404(1)	17.406(1)
$y=1.11$	337.5(1)	0.252(1)	0.439(1)	14.085(1)
$y=1.26$	337.3(1)	0.124(1)	0.459(1)	13.236(1)
$y=1.46$	337.0(1)	0.132(1)	0.465(1)	12.785(1)

which depends only on the fluorine content. The Raman measurements being performed at room temperature, between $300\le\omega\le380$ cm^{-1}, $n(\omega,T)$ is constant (not far from 0.2). The e-ph matrix element, g, depends on frequency and temperature. However, since $T=300$ K and the relevant frequency range is small (80 cm^{-1}), the coupling factor g is assumed to be constant. g has been deduced from the fit of the undoped compound spectrum ($y=0$) to the theoretical Raman scattering intensity, Eq. (8), and is found to be equal to -0.2. The fits of the PAL with variable fluorine content are displayed in Fig. 6. We have determined the number of electronic excitations, $\rho(\omega)$ at ω_0, the frequency ω_0, the factor I_0, and the ratio λ. In the calculation, the value of ω_0 has been constrained by another equation, $\omega_0=\omega_{max}+\Gamma/q$, where ω_{max} is the experimental frequency of the PAL maximum, which can be deduced from the experimental data. The agreement between theory and experiment is quite good, which confirms the choice of the fitting parameters. The parameters I_0, ω_0, and λ and the symmetric factor $|q|$ are listed in Table IV.

The decreasing factor I_0 is mainly due to an increase of the absorption coefficient. The increase of the ratio λ implies an increase of the electronic scattering rate. The number of electronic excitations $\rho(\omega)$ near ω_0 as a function of the fluorine content is shown in Fig. 7. $\rho(\omega_0)$ was extracted from the PAL of the B_{1g} mode localized in the CuO_2 plane; therefore, $\rho(\omega_0)$ represents the electronic excitations near ω_0 which come predominantly from the CuO_2 planes. $\rho(\omega_0)$ increases from $y=0$ to 1.1 and

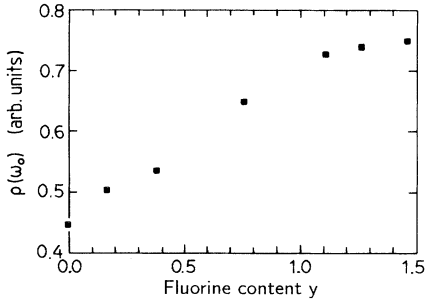

FIG. 7. The number of electronic excitations, $\rho(\omega)$, near ω_0, as a function of the fluorine content.

presents a much smoother increase between $1.1 \leq y \leq 1.5$.

If we can calculate the electronic polarization operator $\Pi(\omega)$ for finite temperature and variable density of carriers, we shall be able to derive the relation between the carrier concentration and $\rho(\omega)$, in an I/M regime where the transition from a Boltzmann to a Fermi gas of carriers may occur with increase of carrier concentration. This calculation involves the electronic damping γ which is large in YBCO materials.[40] To make it tractable, we make several simplifying assumptions. First, we consider the spectrum of carriers as purely two dimensional (2D) and isotropic. Second, the 2D density of single electronic states $\nu(\varepsilon)$ is considered as a constant $\nu(\varepsilon)=\nu(0)$. Finally, we shall only take into account elastic and quasielastic scattering of carriers, for which the energy change is small compared with $k_B T$. Under these assumptions, $\rho(\omega)=A\omega\,\mathrm{Im}[\Pi(\omega)]$ reduces to[41,42]

$$\rho(\omega)=A\int_0^\infty \frac{\omega\gamma(\varepsilon)}{\omega^2+\gamma^2(\varepsilon)}[n(\varepsilon)-n(\varepsilon+\hbar\omega)]\nu(\varepsilon)d\varepsilon \ . \quad (12)$$

Along with the assumption of the energy-independent density of states, we assume also an energy-independent damping γ. The integral over energy reduces to

$$\rho(\omega)=A\nu(0)\frac{\gamma\omega}{\omega^2+\gamma^2}\int_0^\infty [n(\varepsilon)-n(\varepsilon+\hbar\omega)]d\varepsilon \ , \quad (13)$$

where $\nu(0)$ is the $2D$ electronic density of states equal to $m^*/\pi\hbar^2$ (m^* is the effective mass) and γ is the eigenvalue of the quasi-elastic collision integral corresponding to the fluctuations of the electron distribution functions excited by the phonon.

To evaluate this integral, we use the exact Fermi-Dirac distribution function, $n(\varepsilon)=\{\exp[(\varepsilon-\mu)/k_B T]+1\}^{-1}$, which is valid for arbitrary degeneracy of the electron gas. The chemical potential is related to the density of carriers as follows:

$$N_{2D}=\nu(0)\int_0^\infty \left\{\exp\left[\frac{\varepsilon-\mu}{k_B T}\right]+1\right\}^{-1} d\varepsilon \ . \quad (14)$$

N_{2D} represents the free-carrier density of the Cu-O_2 planes. Calculating the integrals (12) and (13) expressing μ in terms of N_{2D}, we get finally

$$\rho(\omega)=A\nu(0)\frac{\gamma\omega}{\omega^2+\gamma^2}\left[\frac{N_{2D}}{\nu(0)}+\hbar\omega-k_B T\ln\left[e^{\hbar\omega/k_B T}+e^{N_{2D}/\nu(0)k_B T}-1\right]\right] . \quad (15)$$

For $\omega_0 \approx 340\ \mathrm{cm}^{-1}$ and $T \approx 300$ K, we have $\hbar\omega \approx 1.7 k_B T$. When $N_{2D}\to 0$, $\rho(\omega_0)\to 0$ and when $N_{2D} \gg \nu(0)k_B T$, $\rho(\omega_0)$ tends to the limit $A\nu(0)\gamma\omega_0^2\hbar/(\gamma^2+\omega_0^2)$. In the framework of this calculation, $\rho(\omega)$ is an increasing function of the free-carrier density, N_{2D}. The increase of $\rho(\omega)$ with increasing fluorine doping, displayed in Fig. 7, points out the free-carrier density enhancement in the CuO_2 planes.

VI. CONCLUSION

X-ray diffraction, magnetic susceptibility, dc conductivity, FIR, and RS measurements have been performed on $YBa_2Cu_3O_6F_y$ pellets with various fluorine dopings, $0 \leq y \leq 1.46$. X-ray diffraction shows that the $YBa_2Cu_3O_6F_y$ compound preserves its tetragonal phase during the fluorination process. Magnetic susceptibility, dc conductivity, and FIR measurements clearly show the occurrence of the I/M transition at $y \approx 0.76$ with the appearance of the superconducting phase at low temperature ($T_c \approx 35$ K). New modes at 485 and 589 cm^{-1} detected in the FIR and RS measurements, respectively, are assigned to the fluorine atoms inserted into the Cu1-Cu1 chains. The FIR studies show the decrease of the ω_{LO}-ω_{TO} frequency spitting related to the intralayer modes involving the atomic vibrations inside the BaO and CuO_2 planes, whereas the ω_{LO}-ω_{TO} splitting related to the interlayer modes, involving the atomic vibrations of the Cu1-Cu2-O4 bonding, increases. We have examined three possible reasons for the change of the ω_{LO}-ω_{TO} splitting with the fluorine doping: charge transfer, the effect of lattice disorder, and the effect of the plasma in ceramics. We have shown that the last two effects are insufficient to explain the ω_{LO}-ω_{TO} splitting changes detected. On the other hand, Raman investigations are consistent with the charge-transfer assumption. Raman spectra show the frequency hardening of the interlayer modes and the frequency softening of the intralayer modes with increasing doping. The former points out the increase of the effective Coulomb forces within the Cu1-O4-Cu2 bonds and the latter, their decrease inside the CuO_2 planes. The phonon line shape of the B_{1g} normal mode related to the CuO_2 planes changes with fluorine doping. By describing its line-shape deformation by the interference between a single phonon state and an electronic continuum, we have extracted the number of electronic excitations $\rho(\omega)$ in the vicinity of ω_0 and show that $\rho(\omega)$ increases with fluorine doping. Using the simplest model of a 2D Fermi gas of carriers, we have related $\rho(\omega)$ to the free-carrier density of the CuO_2 plane and point out the enhancement of the free-carrier density in the CuO_2 planes. The charge transfer is revealed by the increase of the ionic Coulomb interactions within the Cu1-O4-Cu2 interlayer bonds and their decrease and screening by the free-carrier enhancement inside the CuO_2 planes with increasing fluorine doping.

Overall, FIR, RS, dc conductivity, and magnetic susceptibility measurements are coherent and consistent with the occurrence of the charge transfer from the chains to the CuO_2 planes in the vicinity of $y=0.76$, yielding a metallic and superconducting phase in $YBa_2Cu_3O_6F_y$.

ACKNOWLEDGMENTS

The authors are indebted to Dr. N. Bontemps, Dr. P. Monod, and Dr. E. Y. Sherman for many valuable discussions and suggestions. We are grateful to Dr. F. Gervais for fruitful discussions and his programm assistance of the FPSQ model. One of us (V.A.S.) acknowledges the support of the French Government.

*Permanent address: A. F. Ioffe Physical Technical Institute, St. Petersburg 194021, Russia.

[1]M. Stavola, D. M. Krol, S. A. Sunshine, A. Jayarman, G. A. Kourouklis, R. J. Cava, and E. A. Rietman, Phys. Rev. B **36**, 850 (1987).

[2]C. Thomsen, R. Liu, M. Bauer, A. Wittlin, L. Genzel, M. Cardona, E. Schönherr, W. Bauhofer, and W. König, Solid State Commun. **65**, 55 (1988).

[3]M. Hangyo, S. Nakashima, K. Mizogushi, A. Fujii, A. Mitsuichi, and J. Yotsoya, Solid State Commun. **65**, 835 (1988).

[4]G. Burns, F. H. Dacol, C. Field, and F. Holtzberg, Solid State Commun. **75**, 893 (1990).

[5]G. Burns, F. H. Dacol, C. Field, and F. Holtzberg, Solid State Commun. **77**, 367 (1991).

[6]A. Sacuto, M. Balkanski, O. Gorochov, and R. Surryanarayanan, in *Proceedings of the European Material Research Society, Fall Meeting on High T_c Superconductors,* Strasbourg, France, edited by J. Dumas (Elsevier Science, Amsterdam, 1993). J. Alloys Compounds **195**, 359 (1993).

[7]S. Massida, J. Yu, A. J. Freeman, and D. D. Koelling, Phys. Lett. A **122**, 198 (1987).

[8]Y. Tokura, J. B. Torrance, T. C. Huang, and A. I. Nazzal, Phys. Rev. B **38**, 7156 (1988).

[9]J. K. Burdett and G. V. Kulkarni, Phys. Rev. B **40**, 8908 (1989).

[10]S. L. Cooper, A. L. Kotz, M. A. Karlow, M. V. Klein, W. C. Lee, J. Giapintzakis, and D. M. Ginsberg, Phys. Rev. B **45**, 2549 (1992).

[11]S. L. Cooper, P. Nyhus, D. Reznik, M. V. Klein, W. C. Lee, D. M. Ginsberg, B. W. Veal, A. P. Paulikas, and B. Dabrowski, Phys. Rev. Lett. **70**, 1533 (1993).

[12]P. F. Miceli, J. M. Tarascon, L. H. Greene, P. Barboux, F. J. Rotella, and J. D. Jorgensen, Phys. Rev. B **37**, 5932 (1988).

[13]J. D. Jorgensen, B. W. Veal, A. P. Paulikas, L. J. Nowicki, G. W. Crabtree, H. Claus, and W. K. Kwok, Phys. Rev. B **41**, 1863 (1990).

[14]F. Gervais and B. Piriou, Phys. Rev. B **10**, 1642 (1974).

[15]C. Perrin, O. Pena, M. Sergent, P. Christensen, G. Fonteneau, and J. Lucas, Supercond. Sci. Technol. **2**, 35 (1989).

[16]C. Perrin, A. Dinia, O. Pena, M. Sergent, P. Burlet, and J. Rossat-Mignod, Solid State Commun. **76**, 401 (1990).

[17]M. Mokhtari, Ph.D. thesis, Rennes I University, 1993.

[18]L.Genzel, A. Wittlin, M. Bauer, M. Cardona, E. Schönherr, and A. Simon, Phys. Rev. B **40**, 2170 (1989).

[19]M. Bauer, I. B. Ferreira, L. Genzel, M. Cardona, P. Murugaraj, and J. Maier, Solid State Commun. **72**, 551 (1989).

[20]M. K. Crawford, G. Burns, and F. Holtzberg, Solid State Commun. **70**, 557 (1989).

[21]Z. Schlesinger, R. T. Collins, F. Holtzberg, C. Feild, G. Koren, and A. Gupta, Phys. Rev. B **41**, 11 238 (1990); Z. Schlesinger, R. T. Collins, F. Holtzberg, C. Feild, S. H. Blanton, U. Welp, G. W. Crabtree, Y. Fang, and J. Z. Liu, Phys. Rev. Lett. **65**, 801 (1990).

[22]J. Bouvier, N. Bontemps, M. Gabay, M. Nanot, and F. Queyroux, Phys. Rev. B **45**, 8065 (1992).

[23]R. T. Collins, Z. Schlesinger, F. Holtzberg, P. Chaudhari, and C. Feild, Phys. Rev. B **39**, 6571 (1989).

[24]A. El Azrak, R. Nahoum, N. Bontemps, M. Guilloux-Viry, C. Thivet, A. Perrin, S. Labdi, Z. Z. Li, and H. Raffi, Phys. Rev. B **49**, 9846 (1994).

[25]F. Gervais, R. P. S. M. Lobo, C. Allonçon, N. Pellerin, J. M. Bassat, J. P. Loup, and P. Odier, Solid State Commun. **88**, 245 (1993).

[26]R. P. S. M. Lobo, F. Gervais, C. Champeaux, P. Marchet, and A. Catherinot (unpublished).

[27]C. Thomsen, M. Cardona, W. Kress, R. Liu, L. Genzel, M. Bauer, E. Schönherr, and U. Schröder, Solid State Commun. **65**, 1139 (1988).

[28]F. E. Bates, Phys. Rev. B **39**, 322 (1989).

[29]W. Cochran and R. A. Cowley, J. Phys. Chem. Solids **23**, 447 (1962).

[30]L. Landau and E. M. Lifshitz, *Electrodynamics of the Continuous Medium* (Pergamon, London, 1969).

[31]A sudden change had been reported (see Ref. 5) in the Raman phonon spectrum of the $YBa_2Cu_3O_{6+x}$ system at the I/M transition. Unfortunately, these results were in disagreement with the previous measurements (Refs. 1–4,6). We suspect that this drastic change in the Raman spectrum was originating from a phase other than the $YBa_2Cu_3O_6$.

[32]Kyung-Min Ham, R. Sooryakumar, C. Kwon, Q. Li, and T. Venkatesan, Phys. Rev. B **48**, 16 744 (1993).

[33]Kyung-Min Ham, R. Sooryakumar, I. Takeuchi, Z. Trajanovic, C. Kwon, Q. Li, and T. Venkatesan, Phys. Rev. B **50**, 16 598 (1994).

[34]O. V. Misochko and E. Ya. Shermann, Physica C **222**, 219 (1994).

[35]W. Kress, U. Schröder, J. Prade, A. D. Kulkarni, and F. W. de Wette, Phys. Rev. B **38**, 2906 (1988).

[36]M V. Klein, in *Light Scattering in Solids I,* edited by M. Cardona, Topics in Applied Physics, Vol. 8 (Springer, Berlin, 1983), p. 149.

[37]A. Sacuto, C. Julien, V. A. Shchukin, M. Mokhtari, and C. Perrin, Physica C **235-240**, 1293 (1994).

[38]A. Zawadowski and J. Ruvalds, Phys. Rev. Lett. **24**, 1111 (1970).

[39]A. Sacuto, M. Kanehisa, and O. Gorochov, J. Phys. Condens. Matter **6**, 1057 (1994).

[40]A. Virosztek and J Ruvalds, Phys. Rev. B **45**, 347 (1992).

[41]B. L. Al'tshuler, Sov. Phys. JETP **48**, 670 (1978).

[42]I. P. Ipatova, A. V. Subashiev, and V. A. Shchukin, Sov. Phys. Solid State **24**, 1932 (1982).